Journal of Drug Delivery Science and Technology 77 (2022) 103844

Contents lists available at ScienceDirect

Journal of Drug Delivery Science and Technology

journal homepage: www.elsevier.com/locate/jddst

Gelatin methacryloyl/nanosilicate nanocomposite hydrogels encapsulating dexamethasone with a tunable crosslinking density for bone repair

Emine Alarçin [a,*], Ayşe Begüm Dokgöz [a], Zeynep Püren Akgüner [b], Hatice Kübra Seki [a], Ayça Bal-Öztürk [b,c]

[a] Department of Pharmaceutical Technology, Faculty of Pharmacy, Marmara University, Istanbul, Turkey
[b] Department of Stem Cell and Tissue Engineering, Institute of Health Sciences, Istinye University, Istanbul, Turkey
[c] Department of Analytical Chemistry, Faculty of Pharmacy, Istinye University, Zeytinburnu, Turkey

ARTICLE INFO

Keywords:
GelMA
Nanosilicate
Dexamethasone
Nanocomposite hydrogels
Bone repair

ABSTRACT

Despite various strategies have been proposed to accelerate bone regeneration, the treatment of bone defects in critical size still remains a clinical challenge. In this study, we fabricated nanocomposite gelatin methacryloyl (GelMA)/nanosilicate (NS) hydrogels for the delivery of dexamethasone (DEX), and systematically investigated their performance in drug delivery for bone repair. Nanocomposite hydrogels were fabricated by mold casting, and exposed to ultraviolet (UV) light to induce covalent crosslinking. Afterwards, we conducted a systematic characterization study to determine the effects of varying NS concentration, GelMA methacrylation degree and UV exposure time on mechanical, structural, and drug release behaviors of nanocomposite hydrogels. In particular, the higher methacrylation degree of GelMA, longer UV exposure and the presence of NS exhibited gradually enhanced mechanical properties. For instance, the compressive strengths of nanocomposite hydrogels containing 0% (w/v) NS (G0NS120) and 3% (w/v) NS (G3NS120) at 120 s of UV exposure were 194.816 kPa–367.284 kPa ($p < 0.001$), respectively. Similarly, they exhibited higher swelling ratio (%) and slower degradation rate (%) with longer UV exposure and increased NS amount. Nanocomposite hydrogels revealed slower drug release rate due to longer UV exposure and increased NS amount. At day 14 of the release study, 99.53% and 60.687% of DEX were released from G0NS120 and G3NS120, respectively. Particularly, the nanocomposite GelMA/NS hydrogels supported osteoblast adhesion well, and NS and DEX exhibited synergistic effect on osteoblast proliferation with 5.01 fold increase after 7 days of culture. Our results clearly showed that GelMA/NS nanocomposite hydrogels with tunable physiochemical and drug carrier properties could provide a favorable option for accelerating bone repair.

1. Introduction

Bone is a highly dynamic connective tissue with a key role in mechanical support, mobility of body, and blood cell production [1,2]. Bone disorders caused by trauma, osteoporosis, bone infection, tumors, and rheumatic diseases affect more than 20 million people annually worldwide, resulting in substantial pain, reduction in long term quality of life, and economic burden on patients [3,4]. Even though, bone has a significant regeneration capacity, large defects beyond a critical size cannot allow complete healing without orthopedic intervention, and the complete healing of large scale bone defects still remains a major challenge in clinical surgery [2,5,6]. The current approaches for the treatment of critical-size bone defects are the use of autografts and allografts [7]. Despite, autografts are still gold standard for the repair of critical size bone defects, this approach has important shortcomings associated with second surgery, high cost, donor site morbidity, infection, and chronic pain [8,9]. Besides, allografts suffer from shortage of donor, immune rejection, infection, and disease transmission as the second most common treatment option [10]. To address these limitations, a variety of materials including metals (e.g. titanium, magnesium), bioceramics (e.g. hydroxyapatite, beta-tricalcium phosphate), natural (e.g. collagen, hyaluronic acid), and synthetic polymers (e.g. poly(D, L-lactic-glycolic acid), polycaprolactone) or their composites have been proposed to repair critical-sized bone defects [3,9,11]. However, despite recent advances in orthopedics research, adequate healing of bone disorders remains an unsolved clinical challenge due to

* Corresponding author.
E-mail addresses: emine.alarcin@marmara.edu.tr, eminealarcin@gmail.com (E. Alarçin).

https://doi.org/10.1016/j.jddst.2022.103844
Received 12 June 2022; Received in revised form 13 September 2022; Accepted 26 September 2022
Available online 29 September 2022

characteristic drawbacks of these materials.

Hydrogels such as collagen, gelatin, hyaluronic acid and alginate have attracted great interest in bone regeneration due to their distinctive characteristics including high water content, flexibility, porous structure, and biocompatibility. In particular, they could closely mimic physical and chemical properties of the natural extracellular matrix (ECM) of the bone. They are also able to encapsulate bioactive molecules and cells and precisely control the release of entrapped molecule [12–14]. In recent years, among these hydrogels, gelatin methacryloyl (GelMA), photocrosslinkable form of gelatin, is widely used in biomedical applications owing to its biocompatibility and tunable physical properties [15,16]. The physical properties of GelMA hydrogel including degradation, swelling, drug release, and mechanical properties could be precisely control through methacrylation degree of GelMA and UV light exposure time [17].

To date, various nanocomposite hydrogels fabricated by the addition of hydroxyapatite, beta-tricalcium phosphate, bioactive glasses, nanosilicates, graphene oxide, and carbon nanotubes have been widely employed to accelerate the mechanical and osteogenic characteristics of hydrogels [16,18,19]. Among them, currently, nanosilicate (NS) has shown a great potential in bone reconstruction and regeneration [20]. NS ($Na_{0.7}[(Mg_{5.5}Li_{0.3})Si_8O_{20}(OH)_4]_{0.7}$) is a two dimensional smectite clay with around 1 nm in thickness and 20–30 nm in diameter [21]. NS exhibits an anisotropic surface charge distribution with negatively charged flat top and bottom surfaces, and positively charged edges. This unique disk structure allows creating a "house of cards" structure for the formation of a homogeneous colloidal suspension [22–24]. In addition, thanks to its anisotropic surface charge distribution, it could reveal a physically crosslinked network by electrostatic interaction with anionic, cationic, and neutral polymers, resulting in a remarkable increase in mechanical strength and drug release properties avoiding burst release [25–27]. Additionally, it is biocompatible and has generally regarded as safe by The Food and Drug Administration (FDA) [28]. Moreover, it has been demonstrated to achieve osteoinduction and osteogenic differentiation of human mesenchymal stem cells (hMSCs) and adipose stem cells (ASCs) in the absence of growth factors owing to its bioactive degradation products such as lithium, magnesium and orthosilicic acid [29]. Hence, previous studies revealed that nanosilicate incorporated systems could simultaneously enhance bone regeneration. For instance, Dong and coworkers prepared GelMA nanosilicate for extrusion bioprinting, and the rheological properties, the mechanical strength of the hydrogel and osteogenic differentiation of bone marrow mesenchymal stem cell (BMSC) were promoted by the addition of nanosilicate [30]. Roozbahani and coworkers fabricated nanocomposite porous calcium phosphate cements consisting of dexamethasone loaded nanosilicate which resulted remarkably reduced burst release of dexamethasone [31]. Similarly, Liu and coworkers developed BMSCs encapsulated gelatin, alginate, and nanosilicate hydrogel [28]. We have also previously developed silicate based bilayer injectable scaffold for the treatment of nonunion bone defects. The addition of nanosilicate enhanced the rheological properties and the mechanical strength of the hydrogel, and significantly accelerated the growth of the osteogenic cells and endothelial cells *in vitro* [20]. Then, a double layer osteochondral hydrogel was designed by using alginate (Alg)-polyacrylamide (PAAm) and laponite XLS/Alg-PAAm. Results illustrated that mechanical strengthes of hydrogels were increased around 15 times in the presence of 5 wt% nanosilcate. The transition of macrophage polarization also enhanced to the reparative M2 phase [32].

In this study, we developed nanocomposite dexamethasone sodium phosphate (DEX) loaded nanosilicate/GelMA hydrogels to evaluate hybrid NS hydrogels as functional drug carrier in bone repair. To date, some researches have focused to develop gelatin/NS or GelMA/NS nanocomposite hydrogels. However, due to a lack of systematical evaluation of GelMA and nanosilicate nanocomposite hydrogels for drug delivery, drug carrier properties for bone regeneration have not been clearly elucidated to date. Specifically, we have modulated crosslinking density and NS amount of hydrogels to control DEX release. Hence, we performed a detailed and systematic characterization study to evaluate the effect of varying concentration of NS, methacrylation degree of GelMA, and UV crosslinking time on the mechanical, structural, and drug release behavior of nanocomposite hydrogels. We used DEX as a low molecular weight model drug taking advantage of its osteoinductive effect and immunosuppressive activity to eliminate inflammatory responses during bone regeneration. In particular, the local administration of DEX loaded hydrogels could induce bone regeneration by avoiding undesired side effects of a systemic administration of glucocorticoids.

2. Materials and method

2.1. Materials

Dexamethasone sodium phosphate (DEX) was kindly provided by Deva Pharmaceuticals, Turkey, as a gift. The nanosilicate (Laponite XLG) was purchased from BYK Additives & Instruments. Gelatin from porcine skin (type-A, 300 bloom), methacrylic anhydride (MW 154.16), 2-hydroxy-1-[4-(2 hydroxyethoxy) phenyl]-2-methyl-1-propanone (Irgacure 2959) were purchased from Sigma Aldrich. MC3T3-E1 cells (ATCC® CRL-2593) were purchased from ATCC®. Alpha Minimum Essential Medium (MEM α, nucleosides, no ascorbic acid) was purchased from Gibco. Phosphate buffered saline was purchased from Thermofisher. Cell analysis reagents including Live/Dead kit, PrestoBlue, Alexa 488-phalloidin, and 4′,6-diamidino-2-phenylindole (DAPI) were purchased from ThermoFisher (Waltham, MA, USA). All other reagents were analytical grade and purchased from Sigma Aldrich.

2.2. Synthesis and characterization of gelatin methacryloyl

GelMA polymers with two different methacrylation degrees were synthesized using previous protocol (1). In brief, GelMA was prepared by dissolving 10% (w/v) type A porcine skin gelatin in Dulbecco's phosphate buffered saline (DPBS) at 50 °C. Thereafter, methacrylic anhydride (1.25 mL or 5 mL) was added dropwise into the gelatin solution and stirred for 2 h at 50 °C. The reaction was terminated by fivefold dilution with preheated DPBS at 50 °C. Then, the GelMA solution was dialyzed against distilled water using a dialysis tube (12–14 kDa cutoff, Sigma-Aldrich) for 7 days to allow removal of unreacted methacrylic anhydride and impurities. The obtained GelMA solution was frozen at −80 °C followed by lyophilization for 7 days.

To determine the methacrylation of GelMA, ^{1}H NMR spectra were recorded on a Varian UNITY INOVA NMR spectrometer at 40 °C in deuterium oxide and operating frequency was set as 500 MHz. The Fourier transform infrared (FTIR) spectra of unreacted gelatin and GelMA was obtained at wavelength of 400–4000 cm^{-1} by using a FTIR spectrophotometry equipped with ATR sampling accessory (Jasco FT/IR-4600).

2.3. Preparation of GelMA/nanosilicate nanocomposite hydrogels

GelMA/NS composite hydrogels were prepared by mold casting method using a cylindrical polydimethylsiloxane (PDMS) mold followed by UV exposure (Fig. 1). To obtain cylindrical PDMS molds (5 mm diameter), PDMS and curing material (Sylgard 184 silicone elastomer, Dow Corning) were mixed homogenously in a ratio of 10:1. This solution was kept in a vacuum oven for 30 min to remove air bubbles, poured into a Petri dish including a male mold, and left in a vacuum oven for 15 min. Then, it was kept in an oven for 3 h. To produce GelMA/NS hydrogels, nanosilicates with different concentrations including 0%, 1%, 2%, 3%, and 4% (w/v) were dispersed in distilled water including 10 mg/mL DEX and 0.25% (w/v) photoinitiator [2-hydroxy-1-(4-(hydroxyethoxy) phenyl)-2-methyl-1-propanone, Irgacure 2959] for 5 min at 1000 rpm using vortex. GelMA with high (GelMA) or low methacrylation degree ($GelMA_{LOW}$) were added to this dispersion to obtain total 15% (w/v)

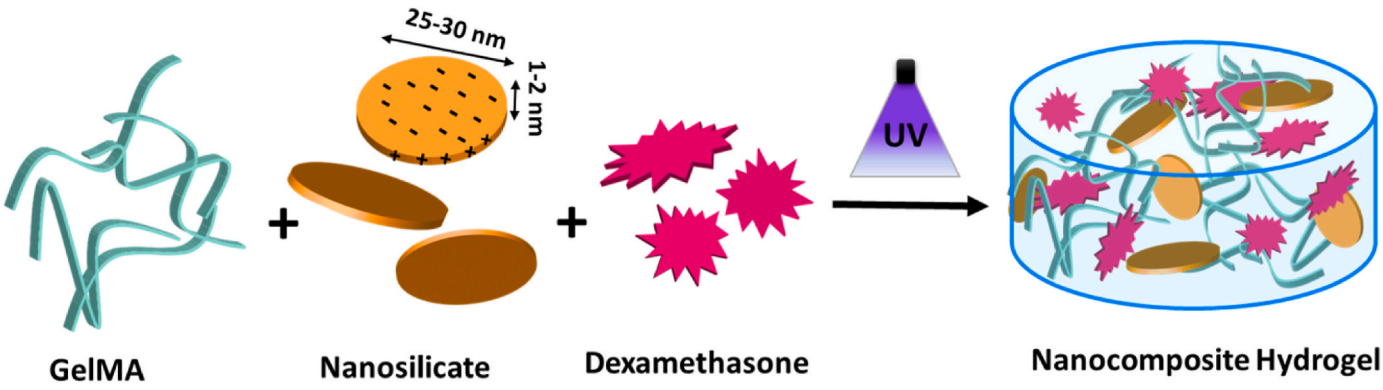

Fig. 1. Schematic of the fabrication of the GelMA/NS/DEX nanocomposite hydrogels.

solid concentration (GelMA and nanosilicate) and stirred at 1000 rpm and 60 °C for further 30 min. Thereafter, 280 μl of GNS mixture was transferred into prepared PDMS mold by pipetting. Immediately after, the hydrogels in PDMS mold were exposed to UV irradiation (360–480 nm, power 5.07 W cm^{-2}, and distance from the light source 8 cm) for 60, 90, or 120 s to determine the effect of exposure time (OmniCure S2000, Excelitas Technologies, Waltham, MA, USA). Nanocomposite hydrogels were coded according to formulation parameters; for instance, hydrogel containing 15% (w/v) GelMA, 0% (w/v) NS, and 60 s UV exposure was coded as G0NS60.

Herein, we first optimized various parameters including MA substitution degree of GelMA, concentration of GelMA (11–15% (w/v)) and NS (1–4% (w/v)), and UV exposure time. Nanocomposite hydrogels containing $GelMA_{LOW}$ and 1%, 2%, 3%, and 4% (w/v) NS were successfully prepared. However, the formulation containing 4% (w/v) NS and GelMA became too viscous before casting to PDMS mold. Therefore, we excluded formulations containing 4% (w/v) nanosilicate from the study for both $GelMA_{LOW}$ and GelMA.

2.4. The Fourier transform infrared spectroscopy analysis

The FTIR analysis was used to determine the chemical interaction between GelMA, nanosilicate, and DEX. FTIR spectra of GelMA, nanosilicate, DEX, their physical mixture, and photocrosslinked GelMA/NS hydrogels were determined at wavelength of 400–4000 cm^{-1} by using a FTIR spectrophotometry equipped with ATR sampling accessory (Jasco FT/IR-4600).

2.5. Scanning Electron Microscopy (SEM) energy dissipative X-ray analysis

The structure and morphology of the composite GelMA/NS hydrogels were determined by Scanning Electron Microscopy (SEM, Zeiss – Evo, MA10). G/NS hydrogels were coated with a thin layer of gold using a sputter coater prior to imaging. Energy Dispersive X-Ray (EDX) analysis was conducted to define the elemental composition of nanocomposite hydrogels.

2.6. Mechanical properties

For mechanical tests, UV crosslinked GelMA/NS hydrogels were soaked into distilled water for 2 h, and the compressive strengths of the samples were determined at cross speed 1 mm s^{-1} and an 80% strain level by using a texture analyzer (TA.XT Plus Texture Analyzer). The compressive modulus was calculated as the slope of the linear region corresponding with 0–10% strain (n = 4).

2.7. Swelling properties

To define swelling properties of GelMA/NS hydrogels, hydrogels were placed in 5 mL of phosphate buffer (pH 7.4) at 37 ± 0.5 °C after UV crosslinking. At predetermined intervals, the hydrogels removed from PBS, the surface water of hydrogels was removed using a filter paper, and then their weight was recorded. The swelling rate was calculated by the ratio between the weight gain and the initial weight (n = 3).

2.8. Degradation properties

To evaluate *in vitro* degradation rate, GelMA/NS were incubated in 10 mL of PBS (pH 7.4) at 37 °C under constant shaking at 100 rpm for up to 4 weeks. At defined time intervals, the hydrogels were removed, rinsed in deionized water, lyophilized and then weighed. PBS was replaced every week. The degradation percentage was reported by the ratio between the weight loss and the initial dry weight using following equation (n = 6):

$$\text{Mass remaining } (\%) = \frac{\text{The final weight of nanocomposite hydrogels}}{\text{The initial weight of nanocomposite hydrogels}} \text{x} 100 \quad (1)$$

2.9. Drug loading

To determine the drug loading efficiency, the prepared dexamethasone loaded hydrogels were cut into small pieces. Then, 10 mL of deionized water was added and stirred at 1000 rpm and 37 °C for 12 h. After complete degradation of hydrogels, obtained solution was filtered, and UV absorbance was determined at 287 nm. Drug loading percentage was reported based on the ratio between drug amounts found in hydrogels and theoretical drug amount (n = 4).

2.10. In vitro drug release

To study *in vitro* drug release, GelMA/NS hydrogels were incubated in 5 mL of PBS at 37.0 °C under constant agitation at 100 rpm for up to 3 weeks. At predetermined time points, the release medium was withdrawn to find the amount of released DEX and replaced with fresh buffer to maintain the sink condition. Immediately after, obtained release medium was filtered and UV absorbance was determined at 287 nm (n = 3).

2.11. In vitro cell culture

MC3T3-E1 preosteoblasts were cultured in α-MEM containing 10% FBS and 1% penicillin-streptomycin and incubated in 5% CO_2 at 37.0 °C. Cell culture medium was replaced every 3 days. Cells were passaged at 80–90% confluence, and passages 2–3 were used in experiments.

Cells (4×10^4 cells/well) were seeded on GelMA/NS nanocomposite hydrogels following UV crosslinking, and then cell adhesion, spreading, and proliferation were evaluated as a function of GelMA, NS, and DEX.

2.11.1. In vitro cell adhesion and spreading studies

To determine cell adhesion and spreading, DAPI and Alexa Fluor 488 phalloidin staining were performed on days 1, 3, and 7 after cell seeding to stain the nuclei and actin fibers of cells according to the manufacturer's instructions. Briefly, cell seeded hydrogels were rinsed in PBS, fixed in paraformaldehyde (4% (w/v)) for 20 min, and then washed with PBS. Triton X-100 (0.05% (v/v)) was applied for 20 min for permeabilization of the cell membrane, and thereafter rabbit serum albumin (5% (w/v)) was applied 1 h to block the membrane. F-actin cytoskeleton stained by incubation in Rhodamine-Phalloidin for 1 h at 37 °C. Subsequently, hydrogels were incubated in DAPI for 30 min at 37 °C for the staining of the nuclei. Immediately after, the stained hydrogels were monitored by fluorescence microscopy (Zeiss AxioScope Z1).

2.11.2. In vitro cell proliferation studies

To evaluate the metabolic activity of cells, PrestoBlue assay was performed according to the manufacturer's instructions at days 1, 3, and 7. In brief, after determined time points, cell seeded hydrogels were incubated in the cell culture medium containing 10% (w/v) PrestoBlue for 1 h at 37 °C. Afterwards, supernatant was collected to measure the fluorescence of the reduced PrestoBlue dye at 570 (excitation) and 600 nm (emission) (Spectroflorometer, Jasco, FP 83009).

2.12. Statistical analysis

Statistical analyses were performed by One-way ANOVA with ±95% confidence interval, and P values < 0.05 were given as statistically significant. The results were reported as mean ± standard deviation (SD).

3. Results and discussion

3.1. Synthesis and characterization of GelMA

$GelMA_{LOW}$ and GelMA were synthesized by modification of gelatin with the reactive methacrylamide (MA) groups using previously reported method (Fig. 2A). The methacrylation degree of GelMA polymer was confirmed by 1H NMR analysis. Two peaks at 5.4 ppm and 5.7 ppm can be attributed to the alkenyl double bond of methacrylate groups conjugated to gelatin (Supp. Fig.1) [33]. Moreover, methacrylation degree of $GelMA_{LOW}$ and GelMA were calculated as 39.4% and 76.8%, respectively. The functional groups of GelMA were determined by FTIR (Fig. 2B). GelMA includes repeating amide bands due to its protein structure. Amide bands in GelMA indicate different vibrational states of peptide bonds. When the spectra of gelatin and low and high methacrylated GelMA were examined, it was observed that some alterations occurred in the C–H stress and flexure regions due to the addition of methacrylate to the lysine groups of gelatin. In FTIR spectrum, the peak observed at 1441 cm^{-1} is known as Amid-III, the result of vibration of N–H bonds and partly C–N bonds. The peak at 1522 cm^{-1}, known as Amide-II, was also obtained due to N–H bonds. At 1628 cm^{-1}, there was Amide-I peak, which shows the vibration of C═O bonds, and the location and intensity of this peak occur as a result of the secondary structure of the gelatin. The peaks seen at 3260 cm^{-1} and 2915 cm^{-1} region were due to O–H and C–H stretching vibrations, respectively. In conclusion, the FTIR results confirmed the successful synthesis of GelMA in accordance with the previous studies [33,34].

3.2. Fabrication of nanocomposite hydrogels

In the preformulation studies, we first determined the compatibility of formulation components including DEX, GelMA and NS using FTIR. An incompatibility problem between formulation ingredients and active agents can lead physical, chemical, and microbiological instability [35].

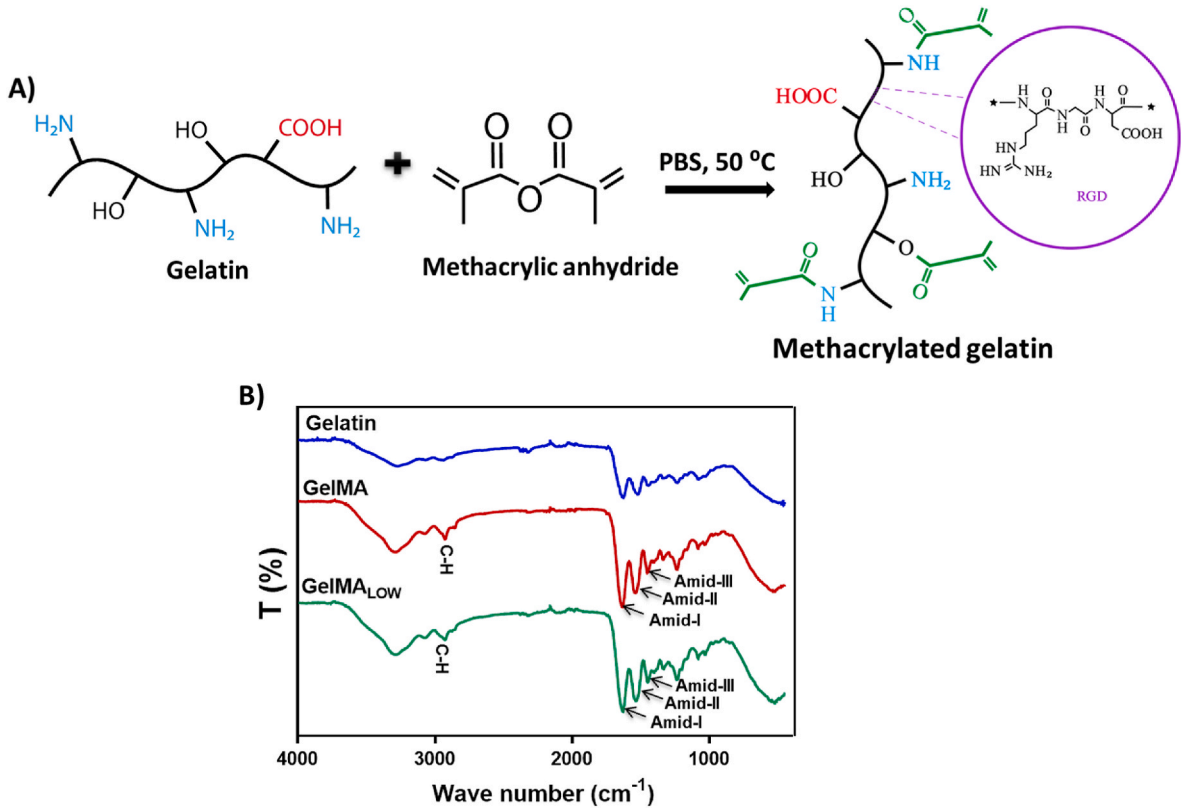

Fig. 2. A) Schematic of the synthesis of GelMA, **B)** FTIR spectra of gelatin and gelatin methacryloyl with low and high methacrylation degree.

Hence, FTIR spectra of DEX, GelMA, NS and their physical mixtures were evaluated, prior to preparation of hydrogels (Fig. 3A, Fig. 3B). Thereafter, the FTIR spectra of hydrogels were analyzed following UV exposure to identify the structure after photocrosslinking. Finally, no incompatibility was detected between formulation components.

According to the obtained IR spectrum of DEX, a wide absorption band was obtained between 3200 and 3500 cm^{-1} depending on the vibration of the hydroxyl groups (Fig. 3A). A band due to C–H strain vibrations in the methyl group was obtained at 2939 cm^{-1}, while a strong absorption band was detected at 1668 cm^{-1} due to C═O strain vibrations. The bands of the phosphate anion in the dexamethasone sodium phosphate structure were determined at 1025, 1031 and 1044 cm^{-1}. The obtained results are consistent with the characteristic spectra for dexamethasone sodium phosphate in the literature [36–38]. Based on IR spectrum of nanosilica, two peaks were detected at 960 and 645 cm^{-1} due to Si–OH, strain in Si–O and stretching in Si–O–Si (Fig. 3A). The peak at 3405 cm^{-1} proved the presence of hydroxyl groups on the nanosilica. The findings are compatible with the characteristic spectra for nanosilica in the literature [39–41]. The IR spectra of DEX, GelMA, NS and their physical mixtures were evaluated (Fig. 3B). Since, the peaks of each component are included in the spectra, it was confirmed that there was no incompatibility between the formulation ingredients and DEX.

Nanocomposite hydrogels were fabricated by mold casting method using a PDMS mold and exposed by UV light (Figs. 1 and 3C). After lyophilization, the IR spectra of nanocomposite hydrogels were analyzed (Fig. 3D). In particular, the amine peaks from GelMA and Si–OH peaks from nanosilicate were determined in the spectra. In addition, there was no difference in the spectra of nanocomposite hydrogels that were UV applied for 90 s and 120 s.

3.3. Mechanical properties of nanocomposite hydrogels

A functional bone construct should be designed to recapitulate load bearing properties of native bone tissue. The stiffness of structure has a vital role in the adhesion, proliferation and differentiation of osteogenic cells. Additionally, hydrogels should maintain their structural integrity during surgical procedures and new tissue formation. Previously, NS has demonstrated a great potential in many aspects of biomedical applications owing to its remarkable structural and mechanical properties. In particular, NS could improve physical properties of GelMA, and the electrostatic interaction between GelMA and NS could enhance physical stability of hydrogel.

The compressive modulus and compressive strength of GelMA hydrogels with or without NS increased gradually with increasing duration of UV exposure such as 60, 90, and 120 s (Fig. 4). For instance, compressive moduli of pristine GelMA hydrogels were found to be 22.73 ± 3.65 kPa (G0NS60) and 39.021 ± 8.68 kPa (G0NS120), for 60 s and 120 s UV exposure. Additionally, compressive moduli improved from 38.53 ± 4.95 kPa (G1NS60) to 56.28 ± 9.82 kPa (G1NS120) for 60 s and 120 s UV exposure (Fig. 4B). Similarly, compressive strengths of those hydrogels increased from 113.325 ± 23.6 kPa (G0NS60) to 194.816 ± 21.71 kPa (G0NS120) for 60 s and 120 s UV exposure (Fig. 4C).

Furthermore, mechanical strength was gradually and significantly enhanced with the increasing NS concentration. For 120 s UV exposure, the compressive moduli increased from 39.021 ± 8.68 kPa (G0NS120) to 74.48 ± 10.61 kPa (G2NS120) with the presence of NS ($p > 0.05$). Similarly, compressive strengths of these hydrogels increased 194.816 kPa (G0NS120) to 333.35 kPa (G2NS120) ($p < 0.01$). However, further increase in NS concentration to 3% (w/v) (G3NS120) slightly enhanced the compressive modulus (79.83 ± 8.89 kPa) and compressive strength (367.29 ± 33.89 kPa) compared to 2% (w/v) NS addition (G2NS120) (p

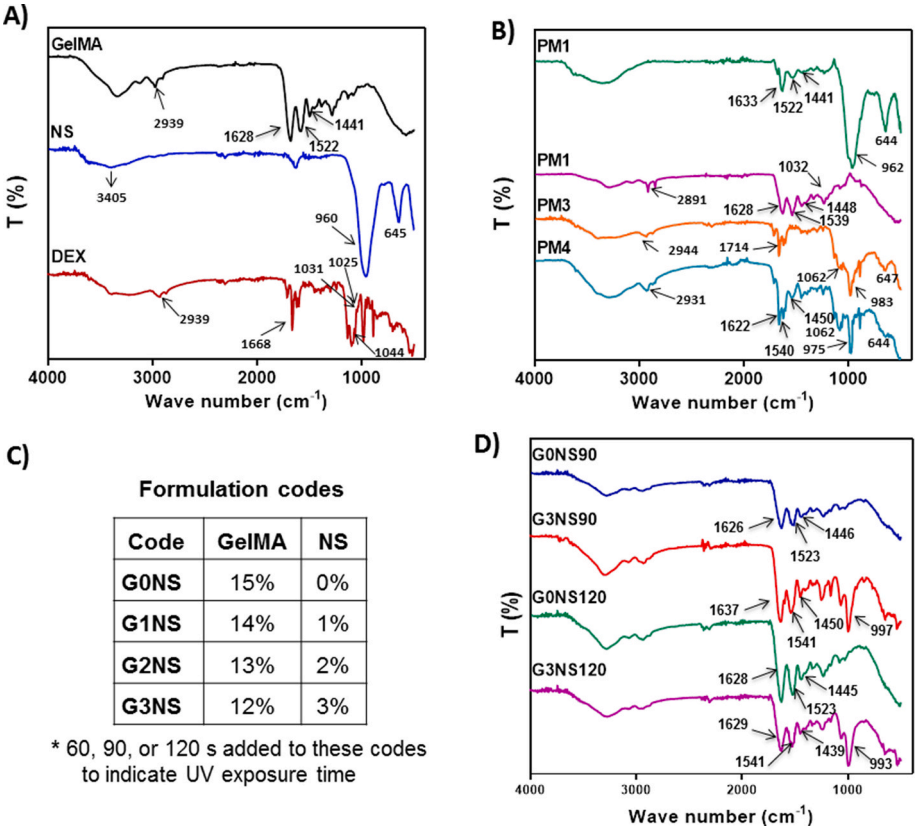

Fig. 3. A) FTIR spectra of GelMA, NS, DEX, **B)** FTIR spectra of physical mixture of formulation components. PM1, PM2, PM3 and PM4 represent GelMA:NS (1:1), GelMA:DEX (1:1), NS:DEX (1:1), and GelMA:NS:DEX (1:1:1), respectively. **C)** Formulation codes for GelMA/NS nanocomposite hydrogels. **D)** FTIR spectra of fabricated nanocomposite hydrogels.

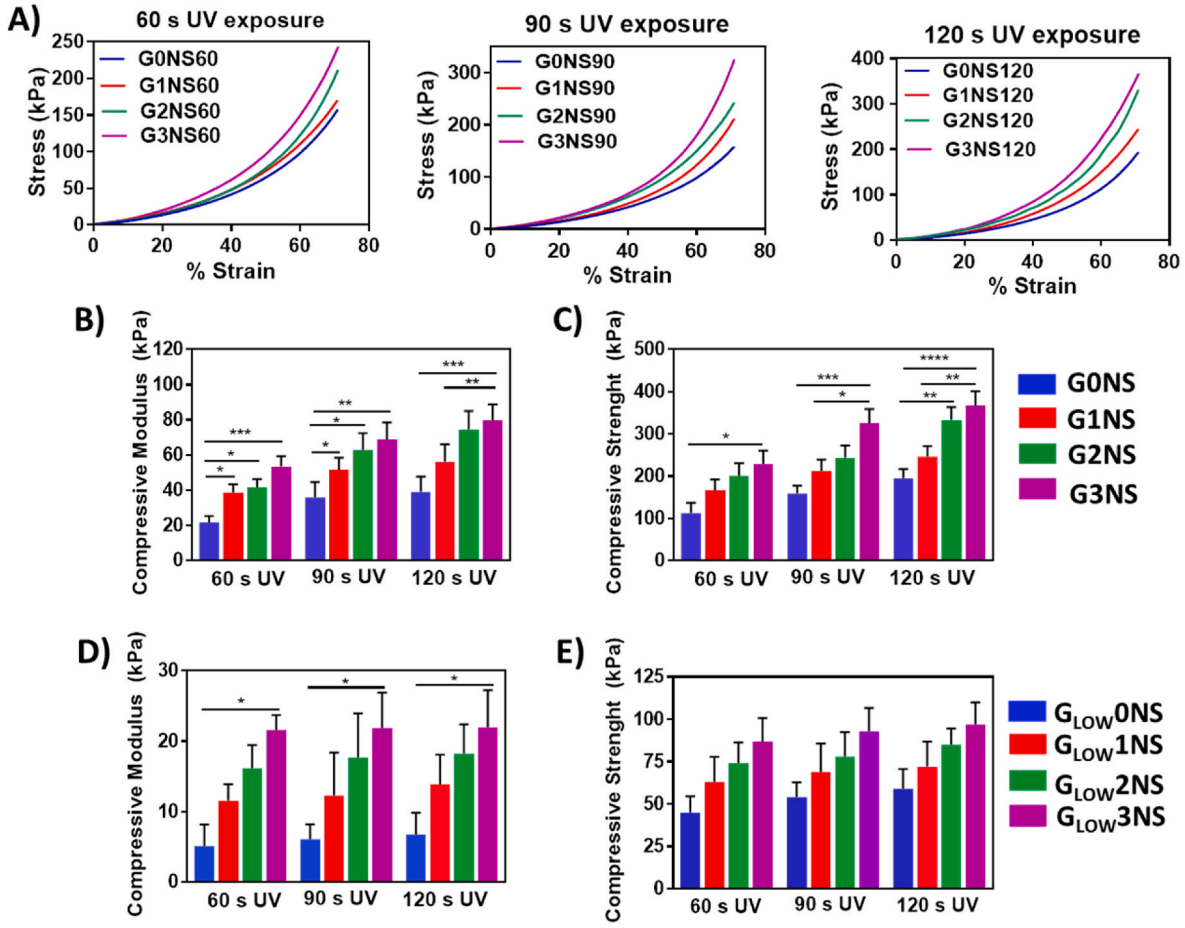

Fig. 4. A) Stress-strain curves for nanocomposite hydrogels applied 60 s, 90 s, and 120 s UV exposure, **B)** Compressive moduli and **C)** Compressive strengths of nanocomposite hydrogels with high methacrylated GelMA and NS, **D)** Compressive moduli and **E)** Compressive strengths of nanocomposite hydrogels with low methacrylated GelMA and NS, (n = 4). (ns > 0.05,*p < 0.05, **p < 0.01; ***p < 0.001; ****p < 0.0001).

> 0.05). In general, an increase in NS amount enhanced the electrostatic interaction between negatively charged NS and positively charged gelatin. Moreover, by the presence of NS in GelMA matrix, mechanical strength and resistance to stress could enhance, polymer yarns and fibers could be more flexible, and also an improved resistance to tension could be obtained. The mechanical pressure could be transmitted directly through the NS and therefore better distributed throughout the entire hydrogel. As a result, NS could increase the stiffness and strength of matrices owing to the improved dispersion of inorganic materials, resulting in a better organic-inorganic interface in hybrid structures [42].

In addition, the NS addition resulted in enhanced mechanical properties in $GelMA_{LOW}$/NS nanocomposite hydrogels (Figs. 4D and E). The compressive moduli were 6.78 ± 3.11 and 21.99 ± 5.35 kPa for G_{LOW}0NS120 and G_{LOW}3NS120, respectively, for 120 s UV exposure. The effect of NS gradually decreased with the increasing UV exposure time. It is also worthy that there was only a slight increase in compressive modulus and compressive strength of hydrogels with $GelMA_{LOW}$ with increasing UV exposure time (p > 0.05). Since $GelMA_{LOW}$ has a small number of methacrylate groups on the polymer backbone, most of these methacrylate groups were able to crosslink within 60 s. Moreover, mechanical strength of hydrogels was significantly enhanced with higher methacrylation degree, as we expected. For instance, after 90 s UV exposure, the compressive moduli of hydrogels fabricated pristine $GelMA_{LOW}$ and GelMA were 6.1 ± 2.12 kPa (G_{LOW}0NS90) and 35.89 ± 8.77 kPa (G0NS90), respectively (p < 0.0001) (Fig. 4B and D). It was attributed to superior covalent crosslinking density of high methacrylated GelMA.

In light of these findings, mechanical properties of nanocomposite hydrogels were governed by methacrylation degree of GelMA, nanosilicate amount, and UV exposure time in accordance with previous literature due to covalent crosslinking density and electrostatic interaction between GelMA and NS. Since, mechanical stability is beneficial to provide effective cellular adhesion and growth, we used hydrogels fabricated by GelMA (with high methacrylation of GelMA) and longer UV exposure including 90 s and 120 s for following experiments.

3.4. SEM and EDX of nanocomposite hydrogels

Herein, the hydrogels gained a more transparent structure in the presence of nanosilicate as seen in Fig. 5in accordance with previous literature [43]. It may be due to suppressed crystallization and the generation of amorphous polymers with the addition of nanosilicate.

In addition to mechanical properties, hydrogels should have an optimal degree of porosity in order to offer sufficient cell growth, nutrient, and vascularization. The morphological features and porosity were analyzed by SEM. As shown in Fig. 5B, all hydrogels in the study presented a highly porous structure. There was no nanosilicate aggregation even in hydrogels with high nanosilicate amount (3% (w/v)). As the NS amount increased, nanosilicate platelets could be identified on the hydrogels. The applied UV time did not provide any alteration in the morphology of the hydrogels. According to EDX analysis silicon and magnesium were detected NS incorporated hydrogels owing to the chemical composition of NS, as we expected (Fig. 5C).

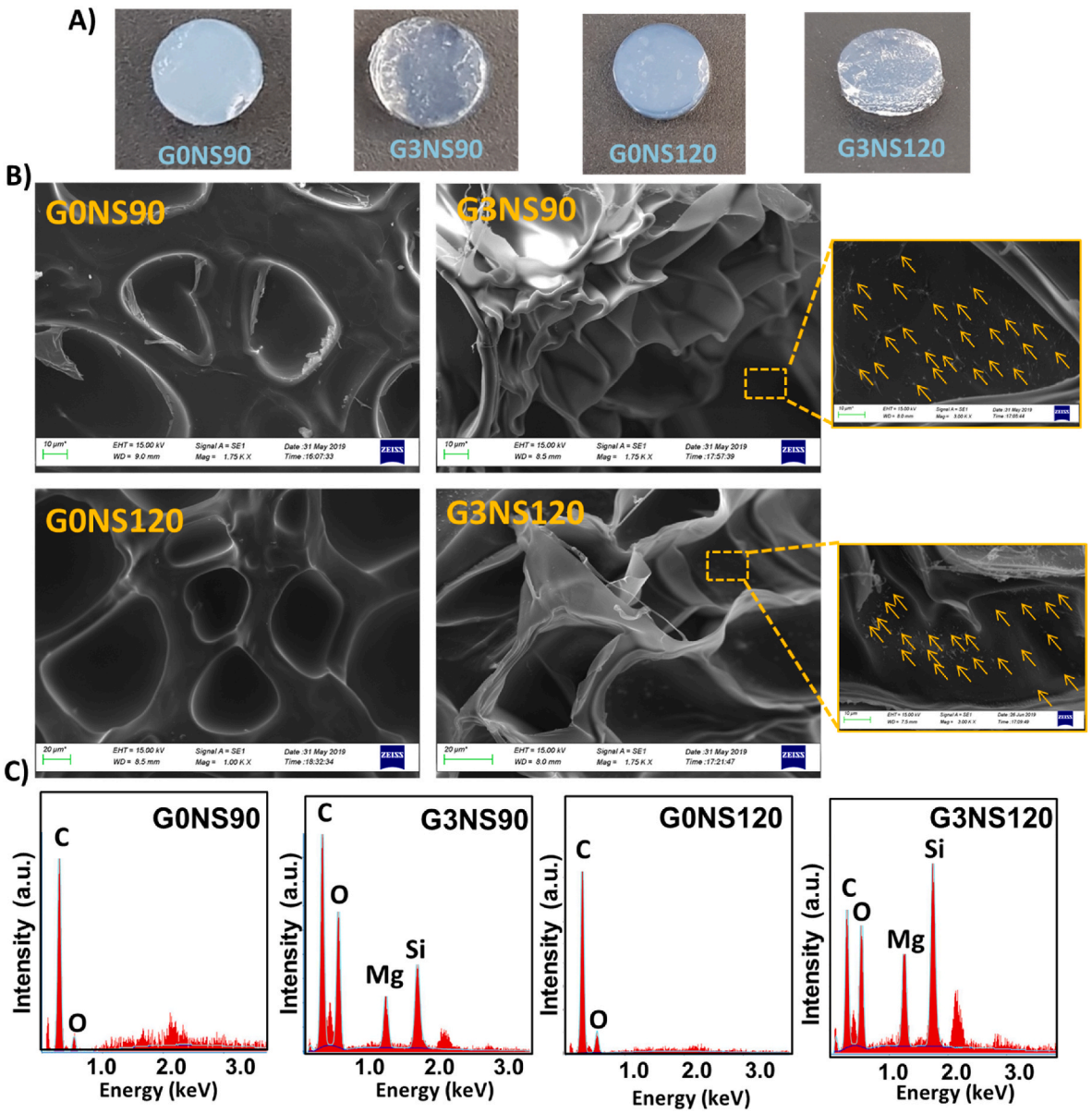

Fig. 5. A) The hydrogels exhibited a more transparent structure after NS addition, **B)** SEM images of nanocomposite hydrogels, **C)** Energy dispersive X-Ray (EDX) analysis of nanocomposite GelMA/NS hydrogels.

3.5. Swelling of nanocomposite hydrogels

The degree of swelling determines the infiltration degree of body fluids into the nanocomposite structure and may have an effect on the release properties of the active substance. In this study, all hydrogels exhibited similar trends with a rapid swelling within the first hour and the presence of swelling equilibrium after 6 h (Fig. 6A). Particularly, the swelling ratio reduced with increasing NS amount, consistent with previous studies [39–41,44]. For instance, after 24 h of incubation, the swelling rate was 453 ± 23.2% for G0NS120 and 336% ± 17.1% for G3NS120 ($P < 0.05$). This reduction can be attributed to electrostatic interaction of GelMA and NS. Additionally, the swelling rate slightly reduced with the increasing duration of UV exposure ($P > 0.05$) due to the presence of covalent interactions.

3.6. Degradation of nanocomposite hydrogels

To obtain effective bone regeneration, the degradation time of hydrogel presents a great importance. Notably, the degradation behavior was mainly governed by nanosilicate amount and duration of UV exposure as shown in Fig. 6B. For instance, the time period for 50% degradation of hydrogels increased, as the amount of nanosilicate and UV exposure became higher (G0NS90: 4 days, G3NS90: 8 days, G0NS120: 6.0 days, and G3NS120: 10 days) due to electrostatic interaction as well as enhanced covalent crosslinking through photopolymerization. Hydrogels with the highest amount of NS and longer UV exposure time (G3NS120) revealed lowest degradation rate with 85.2 ± 5.8% weight remaining after 4 days of incubation. After 7 days of incubation, degradation rates of hydrogels were 17.5 ± 3.1%, 47.1 ± 5.2%, 20.3 ± 3.1%, and 52.7 ± 4.9% for G0NS90, G3NS90, G0NS120, and G3NS120, respectively. The complete degradation of hydrogels was occurred after 13 days, 16 days, 21 days and 24 days for G0NS90, G0NS120, G3NS90, and G3NS120, respectively, mainly dependent to the nanosilicate amount.

3.7. In vitro drug release of nanocomposite hydrogels

To find out the drug entrapment and release capacity of

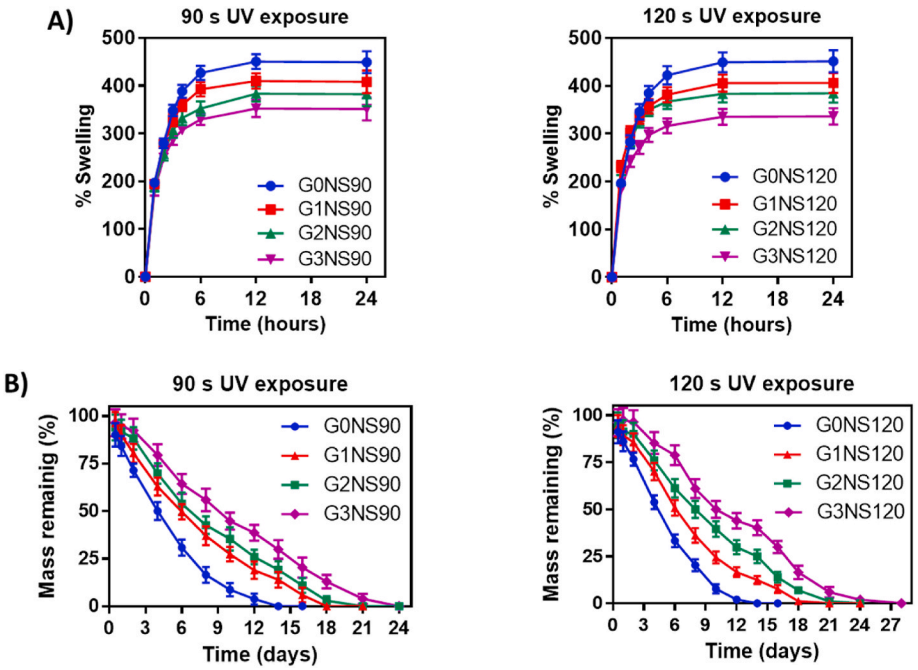

Fig. 6. A) Swelling rate (%) of nanocomposite GelMA/NS hydrogels (n = 3), **B)** Degradation profile of nanocomposite GelMA/NS hydrogels (n = 6).

nanocomposite hydrogels, we used DEX as model drug because of its osteogenic activity. In this study, the loading efficiency of DEX was found to be over 95% for all hydrogels, as we expected.

DEX release from hydrogels was studied in PBS pH 7.4 at 37 °C for 14 days (Fig. 7). For 90 s of UV exposure, 50% DEX was released within the 5, 6, 12, and 48 h from G0NS90, G1NS90, G2NS90, and G3NS90, respectively (Fig. 7A). After 24 h, the released DEX amount was 80.39 ± 8.17% for G0NS90; while it was 41.89 ± 3.69% for G3NS90. At the 14th day, 91.289 ± 7.32%, 83.975 ± 6.84%, and 70.017 ± 7.19% of DEX was released from G1NS90, G2NS90 and G3NS90, respectively. For 120 s of UV exposure, 50% DEX was released within the 6, 14, 24, 96 h from G0NS120, G1NS120, G2NS120, and G3NS120, respectively (Fig. 7B). After 24 h, 74.919 ± 5.17% of DEX was released from G0NS120, whereas only 39.364 ± 4.65% of DEX was released from G3NS120. At the 14th day, 87.901 ± 5.78%, 76.187 ± 7.13%, and 60.687 ± 6.32% of DEX was released from G1NS120, G2NS120 and G3NS120, respectively. However, almost 100% of encapsulated DEX was released after 8 and 10 days from G0NS90 and G0NS120, respectively. The release rate of DEX was governed by nanosilicate amount and UV exposure time. Since UV exposure time increases the degree of covalent binding, the release period of DEX was prolonged with increasing UV exposure time. Moreover, the release rate was also gradually prolonged due to increasing nanosilicate amount attributed to the electrostatic interactions between positively charged gelatin and negatively charged NS.

After defining the release profiles, release kinetics from

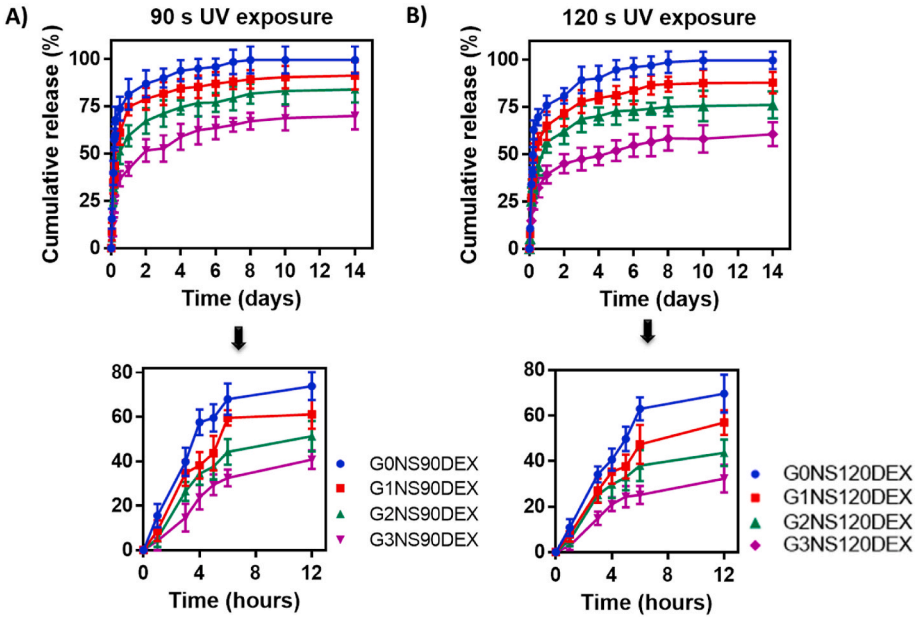

Fig. 7. A) *In vitro* drug release profile of nanocomposite GelMA/NS hydrogels after 90 s UV exposure, **B)** *In vitro* drug release profile of nanocomposite GelMA/NS hydrogels after 120 s UV exposure (n = 3).

nanocomposite hydrogels were calculated using the zero order, first order, Higuchi, Korsmeyer-Peppas and Hixon-Crowel. In general, DEX release from all hydrogels was in accordance with Korsmeyer-Peppas and Higuchi kinetics (Table 1). In hydrogels, the degree of crosslinking and swelling directly affect the drug release, and this could be explained by Korsmeyer-Peppas kinetics. In this study, the r^2 for Korsmeyer Peppas kinetics was higher in hydrogels containing only GelMA with higher swelling rate and crosslinking density. Moreover, "n" was determined as 0.9523 and 0.946 in G0NS90 and G0NS120 coded formulations, respectively, indicating that the release was controlled by swelling and diffusion in these formulations. Notably, the value of "n" gradually decreases as the nanosilicate ratio increases in nanocomposite hydrogels due to decreasing swelling rate of hydrogels with increasing nanosilicate amount. The release mechanism changed from swelling control to diffusion control as the nanosilicate ratio increases. Hence, the value of "n" was found to be lower than 0.5 in formulations containing 3% (w/v) NS indicating the release with the Fick diffusion mechanism. Increasing UV exposure resulted in increased crosslinking density and reduced swelling rate, and therefore, diffusion occurred more dominantly. Due to mentioned reasons, the release mechanism in nanocomposite hydrogels containing nanosilicate has also been found to be compatible with the Higuchi kinetics (diffusion controlled). As a result, swelling is effective for DEX release from formulations containing only GelMA, while diffusion is more effective for those containing nanosilicate.

3.8. In vitro cell studies

A vital requirement to develop a biomaterial for biomedical application is its ability to support cellular adhesion, and proliferation. Cellular adhesion has an important impact on cell spreading, migration, proliferation and differentiation for the ultimate purpose of ECM formation. In this study, MC3T3 preosteoblasts were used to evaluate cell adhesion and proliferation on fabricated nanocomposite hydrogels. To investigate the efficacy of GelMA, NS, and DEX on cellular adhesion, morphology, and spreading, Rhodamine-Phalloidin/DAPI staining was carried out on nanocomposite hydrogels on day 1, 3, and 7. As shown in Fig. 8A, nanocomposite hydrogels did not reveal any cytotoxic effect according to the cellular morphology. Gelatin is known for its good cellular interaction owing to its arginine-glycine-aspartic acid motifs (RGD) for manuplating cell adhesion. Thereby, osteoblast easly adhered to surfaces of hydrogels and elicit cellular spreading. Notably, cellular spreading enhanced in the presence of DEX, NS, and NS-DEX. According to the fluorescence microscopy images, the osteoblast cells spread after 3 and 7 days in culture.

To investigate the mitochondrial activity and proliferation of osteoblast cells on nanostructures, PrestoBlue assay was conducted. The PrestoBlue results indicated that the proliferation of osteoblasts gradually and significantly enhanced over the 1, 3, and 7 days in culture (Fig. 8B). For nanocomposite hydrogels prepared with pristine GelMA, after 7 days of culture, the cell proliferation revealed 3.65 and 3.93 fold increase for G0NS120 and G0NSDEX120, respectively. The addition of NS in G3NS120 provided a significant increase (around 4.65 fold) in the proliferation rate of osteoblast cells after 7 days of culture due to positive effect of degradation product of NS ($p < 0.001$). In particular, the effect of NS on osteoblast proliferation was superior compared to DEX after 3, and 7 days of culture. For instance, after 7 days, the proliferation rate was increased 3.92 and 4.65 fold for G0NSDEX120 and G3NS120, respectively. Overall, GelMA and NS could improve osteoblast adhesion in the presence of any osteinductive factor. The release of DEX also enhanced proliferation of osteoblasts owing to its osteoinductive effect, as we expected. Specifically, we can speculate that NS and DEX provide synergistic effect on osteoblast proliferation which resulted in 5.01 fold increase in the proliferation rate of cells on G3NS120DEX after 7 days.

Taken together, acording to cell culture studies NS incorporated hydrogels (without any osteoinductive agent) could promote cellular interactions and proliferation with no adverse effect. In addition, NS and DEX free pristine GelMA hydrogels (G0NS120) showed a good cell spreading and proliferation. It is well known that GelMA has the bioactive RGD motifs and matrix metalloproteinase (MMP) sensitive motifs which can accelerate cell attachment, proliferation and differentiation [45,46]. NS incorporated hydrogels G3NS120 revealed significantly enhanced cell spreading and proliferation, as we expected. In particular, NS could exhibit osteogenic properties even in the absence of osteoinductive agents owing its structural components such as lithium, magnesium and orthosilicic acid [29]. Lithium could inhibit glycogen synthase kinase-3β and accelerate activity of Wnt/β-catenin signaling pathway [47,48], while orthosilicic acid could accelarate the expression of ALP, COL1 and OCN to enhance osteogenesis [49,50]. Magnesium could promote cellular adhesion, osteogenic differention and also angiogenesis, hence lead functional bone regeneration [51,52]. Also, NS affected cell adhesion and proliferation indirectly owing to remarkebly enhanced mechanical properties of NS containing hydrogels. Importantly, the sustained release of DEX resulted in better cellular spreading and proliferation in GelMA based or GelMA-NS based constructs due to its osteoinductive effect and immunosuppressive activity to eliminate the inflammatory responses during bone regeneration.

Table 1
In vitro release kinetic parameters for GelMA/NS nanocomposite hydrogels.

Code	Zero order	First order	Korsmeyer-Peppas		Higuchi	Hixson-Crowell
	r^2	r^2	r^2	n	r^2	r^2
G0NS90	0.9895	0.9705	0.9901	0.9523	0.9405	0.9833
G1NS90	0.7659	0.8179	0.8919	0.8142	0.9125	0.8033
G2NS90	0.6691	0.7832	0.7995	0.7222	0.8927	0.7454
G3NS90	0.6801	0.7915	0.7924	0.4832	0.8649	0.7554
G0NS120	0.9921	0.9781	0.9933	0.946	0.9411	0.9876
G1NS120	0.7106	0.8325	0.865	0.6519	0.9201	0.7935
G2NS120	0.6573	0.785	0.7851	0.5564	0.8834	0.744
G3NS120	0.7168	0.8173	0.7724	0.388	0.8815	0.7853

4. Conclusion

In this study, we have systematically optimized GelMA/NS hydrogels for the delivery of dexamethasone as a model drug and performed initial cell characterization studies. We prepared nanocomposite hydrogels by mold casting and crosslinked under UV exposure to induce covalent crosslinking. Then, we conducted a systematic and detailed *in vitro* characterization with varying concentration of NS, methacrylation degree of GelMA, and UV crosslinking time to determine their effect on mechanical, structural, and drug release behavior of nanocomposite hydrogels. Notably, the higher methacrylation degree of GelMA, longer UV exposure time and the addition of NS resulted in gradually accelerated mechanical properties, as we expected. The swelling rate of nanocomposite hydrogels was reduced while degradation period was increased due to longer UV exposure time and increased NS amount. Furthermore, slower drug release rate was exhibited with longer UV exposure time and/or increased NS amount. These findings clearly demonstrated the effect of UV crosslinking density and NS amount due to its unique structural features. Finally, the nanocomposite GelMA/NS hydrogels showed favorable adhesion of osteoblastic cells, and NS and DEX achieve synergistic effect on osteoblast proliferation which resulted in 5.01 fold increase in the proliferation rate of cells after 7 days of culture. The obtained results showed that GelMA/NS nanocomposite hydrogels with tunable physiochemical and drug carrier properties could present a beneficial option in bone repair.

Declaration of competing interest

The authors declare that they have no known competing financial interests or personal relationships that could have appeared to influence

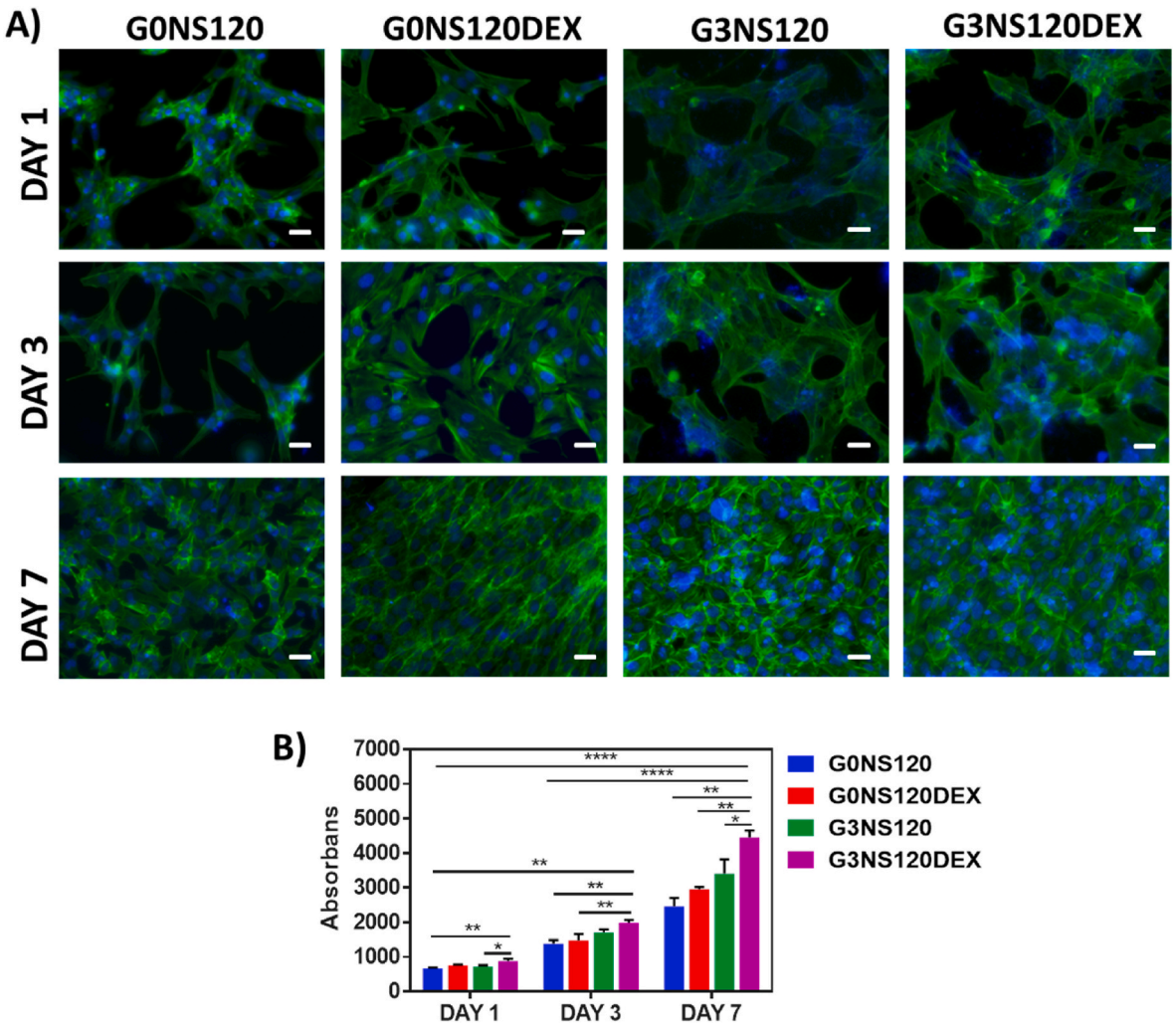

Fig. 8. *In vitro* cell adhesion on GelMA/NS nanocomposite hydrogels on day 1, 3, and 7: A) GelMA/NS nanocomposite scaffolds supported osteoblast adhesion and spreading as determined by Phalloidin/DAPI staining (n = 3). B) The PrestoBlue results of the proliferation of cells seeded on nanocomposite GelMA/NS hydrogels over 1, 3, 5 and 7 days in culture (n = 6). Scale bar: 50 μm. (ns > 0.05,*p < 0.05, **p < 0.01; ***p < 0.001; ****p < 0.0001).

the work reported in this paper.

Data availability

Data will be made available on request.

Acknowledgments

This study was funded by the Scientific and Technological Research Council of Turkey (TÜBİTAK) (Grant Number 112S365). We would like to thank to Deva Pharmaceuticals, Turkey for providing DEX as a gift.

Appendix A. Supplementary data

Supplementary data to this article can be found online at https://doi.org/10.1016/j.jddst.2022.103844.

References

[1] P. Bhattacharjee, B. Kundu, D. Naskar, H.-W. Kim, T.K. Maiti, D. Bhattacharya, S. C. Kundu, Silk scaffolds in bone tissue engineering: an overview, Acta Biomater. 63 (2017) 1–17.
[2] X. Xue, Y. Hu, Y. Deng, J. Su, Recent advances in design of functional biocompatible hydrogels for bone tissue engineering, Adv. Funct. Mater. 31 (19) (2021), 2009432.
[3] T.-M. De Witte, L.E. Fratila-Apachitei, A.A. Zadpoor, N.A. Peppas, Bone tissue engineering via growth factor delivery: from scaffolds to complex matrices, Regenerat. Biomater. 5 (4) (2018) 197–211.
[4] H. Qu, H. Fu, Z. Han, Y. Sun, Biomaterials for bone tissue engineering scaffolds: a review, RSC Adv. 9 (45) (2019) 26252–26262.
[5] G. Turnbull, J. Clarke, F. Picard, P. Riches, L. Jia, F. Han, B. Li, W. Shu, 3D bioactive composite scaffolds for bone tissue engineering, Bioact. Mater. 3 (3) (2018) 278–314.
[6] G.L. Koons, M. Diba, A.G. Mikos, Materials design for bone-tissue engineering, Nat. Rev. Mater. 5 (8) (2020) 584–603.
[7] H. Amirazad, M. Dadashpour, N. Zarghami, Application of decellularized bone matrix as a bioscaffold in bone tissue engineering, J. Biol. Eng. 16 (1) (2022) 1–18.
[8] G. Zhu, T. Zhang, M. Chen, K. Yao, X. Huang, B. Zhang, Y. Li, J. Liu, Y. Wang, Z. Zhao, Bone physiological microenvironment and healing mechanism: basis for future bone-tissue engineering scaffolds, Bioact. Mater. 6 (11) (2021) 4110–4140.
[9] Z. Peng, T. Zhao, Y. Zhou, S. Li, J. Li, R.M. Leblanc, Bone tissue engineering via carbon-based nanomaterials, Adv. Healthcare. Mater. 9 (5) (2020), 1901495.
[10] S. Bose, N. Sarkar, Natural medicinal compounds in bone tissue engineering, Trends Biotechnol. 38 (4) (2020) 404–417.
[11] S.P. Malliappan, A.A. Yetisgin, S.B. Sahin, E. Demir, S. Cetinel, Bone Tissue Engineering: Anionic Polysaccharides as Promising Scaffolds, Carbohydrate Polymers, 2022, 119142.
[12] T. Pan, W. Song, H. Xin, H. Yu, H. Wang, D. Ma, X. Cao, Y. Wang, MicroRNA-activated hydrogel scaffold generated by 3D printing accelerates bone regeneration, Bioact. Mater. 10 (2022) 1–14.
[13] X. Wang, J. Fang, W. Zhu, C. Zhong, D. Ye, M. Zhu, X. Lu, Y. Zhao, F. Ren, Bioinspired highly anisotropic, ultrastrong and stiff, and osteoconductive mineralized wood hydrogel composites for bone repair, Adv. Funct. Mater. 31 (20) (2021), 2010068.
[14] Y. Xiong, Y. Xiong, Applications of bone regeneration hydrogels in the treatment of bone defects: a review, J. Mater. Sci. (2022) 1–27.

[15] Y. Piao, H. You, T. Xu, H.-P. Bei, I.Z. Piwko, Y.Y. Kwan, X. Zhao, Biomedical applications of gelatin methacryloyl hydrogels, Eng. Regenerat. 2 (2021) 47–56.
[16] M.A. Sakr, K. Sakthivel, T. Hossain, S.R. Shin, S. Siddiqua, J. Kim, K. Kim, Recent trends in gelatin methacryloyl nanocomposite hydrogels for tissue engineering, J. Biomed. Mater. Res. 110 (3) (2022) 708–724.
[17] B. Cecen, A. Bal-Ozturk, G. Yasayan, E. Alarcin, P. Kocak, R. Tutar, L.D. Kozaci, S. R. Shin, A.K. Miri, Selection of natural biomaterials for micro-tissue and organ-on-chip models, J. Biomed. Mater. Res. 110 (5) (2022) 1147–1165.
[18] F. Wahid, X.-J. Zhao, S.-R. Jia, H. Bai, C. Zhong, Nanocomposite hydrogels as multifunctional systems for biomedical applications: current state and perspectives, Compos. B Eng. 200 (2020), 108208.
[19] M. Mehrali, A. Thakur, C.P. Pennisi, S. Talebian, A. Arpanaei, M. Nikkhah, A. Dolatshahi-Pirouz, Nanoreinforced hydrogels for tissue engineering: biomaterials that are compatible with load-bearing and electroactive tissues, Adv. Mater. 29 (8) (2017), 1603612.
[20] E. Alarçin, T.Y. Lee, S. Karuthedom, M. Mohammadi, M.A. Brennan, D.H. Lee, A. Marrella, J. Zhang, D. Syla, Y.S. Zhang, Injectable shear-thinning hydrogels for delivering osteogenic and angiogenic cells and growth factors, Biomater. Sci. 6 (6) (2018) 1604–1615.
[21] N. Rajabi, M. Kharaziha, R. Emadi, A. Zarrabi, H. Mokhtari, S. Salehi, An adhesive and injectable nanocomposite hydrogel of thiolated gelatin/gelatin methacrylate/Laponite® as a potential surgical sealant, J. Colloid Interface Sci. 564 (2020) 155–169.
[22] H. Tomás, C.S. Alves, J. Rodrigues, Laponite®, A key nanoplatform for biomedical applications? Nanomed. Nanotechnol. Biol. Med. 14 (7) (2018) 2407–2420.
[23] C.R.F. Junior, R.d.S. Fernandes, M.R. de Moura, F.A. Aouada, On the preparation and physicochemical properties of pH-responsive hydrogel nanocomposite based on poly (acid methacrylic)/laponite RDS, Mater. Today Commun. 23 (2020), 100936.
[24] C. Boyer, L. Figueiredo, R. Pace, J. Lesoeur, T. Rouillon, C. Le Visage, J.-F. Tassin, P. Weiss, J. Guicheux, G. Rethore, Laponite nanoparticle-associated silated hydroxypropylmethyl cellulose as an injectable reinforced interpenetrating network hydrogel for cartilage tissue engineering, Acta Biomater. 65 (2018) 112–122.
[25] G. Lokhande, J.K. Carrow, T. Thakur, J.R. Xavier, M. Parani, K.J. Bayless, A. K. Gaharwar, Nanoengineered injectable hydrogels for wound healing application, Acta Biomater. 70 (2018) 35–47.
[26] A.K. Gaharwar, L.M. Cross, C.W. Peak, K. Gold, J.K. Carrow, A. Brokesh, K. A. Singh, 2D nanoclay for biomedical applications: regenerative medicine, therapeutic delivery, and additive manufacturing, Adv. Mater. (2019), 1900332.
[27] A. Sheikhi, S. Afewerki, R. Oklu, A.K. Gaharwar, A. Khademhosseini, Effect of ionic strength on shear-thinning nanoclay-polymer composite hydrogels, Biomater. Sci. 6 (8) (2018) 2073–2083.
[28] B. Liu, J. Li, X. Lei, S. Miao, S. Zhang, P. Cheng, Y. Song, H. Wu, Y. Gao, L. Bi, Cell-loaded injectable gelatin/alginate/LAPONITE® nanocomposite hydrogel promotes bone healing in a critical-size rat calvarial defect model, RSC Adv. 10 (43) (2020) 25652–25661.
[29] A.K. Gaharwar, S.M. Mihaila, A. Swami, A. Patel, S. Sant, R.L. Reis, A.P. Marques, M.E. Gomes, A. Khademhosseini, Bioactive silicate nanoplatelets for osteogenic differentiation of human mesenchymal stem cells, Adv. Mater. 25 (24) (2013) 3329–3336.
[30] L. Dong, Z. Bu, Y. Xiong, H. Zhang, J. Fang, H. Hu, Z. Liu, X. Li, Facile extrusion 3D printing of gelatine methacrylate/Laponite nanocomposite hydrogel with high concentration nanoclay for bone tissue regeneration, Int. J. Biol. Macromol. 188 (2021) 72–81.
[31] M. Roozbahani, M. Kharaziha, Dexamethasone loaded Laponite®/porous calcium phosphate cement for treatment of bone defects, Biomed. Mater. 14 (5) (2019), 055008.
[32] E. Saygili, P. Saglam-Metiner, B. Cakmak, E. Alarcin, G. Beceren, P. Tulum, Y.-W. Kim, K. Gunes, G.G. Eren-Ozcan, D. Akakin, Bilayered laponite/alginate-poly (acrylamide) composite hydrogel for osteochondral injuries enhances macrophage polarization: an in vivo study, Mater. Sci. Eng. C (2022), 112721.
[33] T.D. Usal, D. Yucel, V. Hasirci, A novel GelMA-pHEMA hydrogel nerve guide for the treatment of peripheral nerve damages, Int. J. Biol. Macromol. 121 (2019) 699–706.
[34] K.R. Mamaghani, S.M. Naghib, A. Zahedi, M. Mozafari, Synthesis and microstructural characterization of GelMa/PEGDA hybrid hydrogel containing graphene oxide for biomedical purposes, Mater. Today Proc. 5 (7) (2018) 15635–15644.
[35] G. Yaşayan, G. Karaca, Z.P. Akgüner, A. Bal Öztürk, Chitosan/collagen composite films as wound dressings encapsulating allantoin and lidocaine hydrochloride, International Journal of Polymeric Mater. Polym. Biomater. 70 (9) (2021) 623–635.
[36] P.K. Sahoo, H.S. Panda, D. Bahadur, Studies on the stability and kinetics of drug release of dexamethasone phosphate intercalated layered double hydroxides nanohybrids, Mater. Chem. Phys. 142 (1) (2013) 106–112.
[37] W.-R. Wang, A. Li, W. Mei, R.-R. Zhu, K. Li, X.-Y. Sun, Y.-C. Qian, S.-L. Wang, Dexamethasone sodium phosphate intercalated layered double hydroxides and their therapeutic efficacy in a murine asthma model, RSC Adv. 5 (30) (2015) 23826–23834.
[38] N. Khoshnood, A. Zamanian, A. Massoudi, Mussel-inspired surface modification of titania nanotubes as a novel drug delivery system, Mater. Sci. Eng. C 77 (2017) 748–754.
[39] J.R. Xavier, T. Thakur, P. Desai, M.K. Jaiswal, N. Sears, E. Cosgriff-Hernandez, R. Kaunas, A.K. Gaharwar, Bioactive nanoengineered hydrogels for bone tissue engineering: a growth-factor-free approach, ACS Nano 9 (3) (2015) 3109–3118.
[40] J.A. Sowjanya, J. Singh, T. Mohita, S. Sarvanan, A. Moorthi, N. Srinivasan, N. Selvamurugan, Biocomposite scaffolds containing chitosan/alginate/nano-silica for bone tissue engineering, Colloids Surf. B Biointerfaces 109 (2013) 294–300.
[41] M. Ghadiri, W. Chrzanowski, W.H. Lee, A. Fathi, F. Dehghani, R. Rohanizadeh, Physico-chemical, mechanical and cytotoxicity characterizations of Laponite®/alginate nanocomposite, Appl. Clay Sci. 85 (2013) 64–73.
[42] Y. Ding, Q. Yao, W. Li, D.W. Schubert, A.R. Boccaccini, J.A. Roether, The evaluation of physical properties and in vitro cell behavior of PHB/PCL/sol–gel derived silica hybrid scaffolds and PHB/PCL/fumed silica composite scaffolds, Colloids Surf. B Biointerfaces 136 (2015) 93–98.
[43] A.K. Gaharwar, V. Kishore, C. Rivera, W. Bullock, C.J. Wu, O. Akkus, G. Schmidt, Physically crosslinked nanocomposites from silicate-crosslinked PEO: mechanical properties and osteogenic differentiation of human mesenchymal stem cells, Macromol. Biosci. 12 (6) (2012) 779–793.
[44] Y. Li, D. Maciel, H. Tomás, J. Rodrigues, H. Ma, X. Shi, pH sensitive Laponite/alginate hybrid hydrogels: swelling behaviour and release mechanism, Soft Matter 7 (13) (2011) 6231–6238.
[45] Z. Yuan, X. Yuan, Y. Zhao, Q. Cai, Y. Wang, R. Luo, S. Yu, Y. Wang, J. Han, L. Ge, Injectable GelMA cryogel microspheres for modularized cell delivery and potential vascularized bone regeneration, Small 17 (11) (2021), 2006596.
[46] S. Buyuksungur, V. Hasirci, N. Hasirci, 3D printed hybrid bone constructs of PCL and dental pulp stem cells loaded GelMA, J. Biomed. Mater. Res. 109 (12) (2021) 2425–2437.
[47] H. Zhou, G. Jiao, M. Dong, H. Chi, H. Wang, W. Wu, H. Liu, S. Ren, M. Kong, C. Li, Orthosilicic acid accelerates bone formation in human osteoblast-like cells through the PI3K–Akt–mTOR pathway, Biol. Trace Elem. Res. 190 (2) (2019) 327–335.
[48] M. Dong, G. Jiao, H. Liu, W. Wu, S. Li, Q. Wang, D. Xu, X. Li, H. Liu, Y. Chen, Biological silicon stimulates collagen type 1 and osteocalcin synthesis in human osteoblast-like cells through the BMP-2/Smad/RUNX2 signaling pathway, Biol. Trace Elem. Res. 173 (2) (2016) 306–315.
[49] T.-b. Huang, Y.-z. Li, K. Yu, Z. Yu, Y. Wang, Z.-w. Jiang, H.-m. Wang, G.-l. Yang, Effect of the Wnt signal-RANKL/OPG axis on the enhanced osteogenic integration of a lithium incorporated surface, Biomater. Sci. 7 (3) (2019) 1101–1116.
[50] K. Hurle, F.R. Maia, V.P. Ribeiro, S. Pina, J.M. Oliveira, F. Goetz-Neunhoeffer, R. L. Reis, Osteogenic lithium-doped brushite cements for bone regeneration, Bioact. Mater. (2021).
[51] X. Zhang, P. Huang, G. Jiang, M. Zhang, F. Yu, X. Dong, L. Wang, Y. Chen, W. Zhang, Y. Qi, A novel magnesium ion-incorporating dual-crosslinked hydrogel to improve bone scaffold-mediated osteogenesis and angiogenesis, Mater. Sci. Eng. C 121 (2021), 111868.
[52] Y. Lai, Y. Li, H. Cao, J. Long, X. Wang, L. Li, C. Li, Q. Jia, B. Teng, T. Tang, Osteogenic magnesium incorporated into PLGA/TCP porous scaffold by 3D printing for repairing challenging bone defect, Biomaterials 197 (2019) 207–219.